Supporting Information (SI)

A Multi-Responsive pH Stable-MOF for Prevalent Hg(I), Hg(II) and Organochlorine Pesticide Detection

Janaki Behera[a], Supriya Mondal[a], Arun K. Manna[b], and Madhab C. Das [a]*

[a]*Department of Chemistry, Indian Institute of Technology Kharagpur, Kharagpur-721302, India*
[b]*Department of Chemistry, Indian Institute of Technology Tirupati, Tirupati, Andhra Pradesh 517619, India*

**E-mail: mcdas@chem.iitkgp.ac.in*
Homepage: https://www.chemiitkgp-mcdaslab.com/

Physical Measurements. The single-crystal XRD diffraction data were collected at 120 K on a Bruker AXS (D8 Quest System) X-ray diffractometer, and Rigaku XtaLAB Synergy equipped with a PHOTON 100 CMOS detector using graphite-monochromated *Mo-*K_α radiation (0.71073 Å). PXRD patterns were recorded using *Cu-*K_α radiation (1.5418 Å) on a Bruker D8 Advance diffractometer. Thermogravimetric analysis (TGA) was performed using a TG 209 *F3* Tarsus (Netzsch), and the sample was heated from room temperature to 800 °C at a rate of 10 °C min^{-1} under N_2 atmosphere. The IR spectra were recorded in the range of 4000-400 cm^{-1} on a Perkin-Elmer RX1 spectrophotometer. The morphology of as-synthesized single crystals of **IITKGP-80** MOF was observed by CarlZeiss MERLIN field-emission scanning electron microscopy (FESEM, JSM 6700F) at an acceleration voltage of 15 kV.

Computational Models and Methods:

Solvated geometries of all the pesticides including H_2TTDC in water medium were fully optimized without any constraints within density functional theory (DFT) adopting dispersion and long-range corrected range-separated hybrid (RSH) ωB97X-D exchange-correlation functional[1] and split-valence triple-zeta polarized 6-311++G(d,p) basis set for all elements. Initial geometry of the MOF for modelling the DCN interaction was extracted from the corresponding X-Ray crystal structure data. Subsequently, the positions of all hydrogen atoms including the adsorbed DCN were only relaxed using spin-polarized DFT (see **Figure S26** for the optimized structure). Both intrachain ferromagnetic (FM) and antiferromagnetic (AFM) spin configurations were considered for identifying the minimum energy magnetic ground-state. Polar solvent effects were accounted for through polarizable continuum model in its default integral-equation formalism with water dielectric.[2] Time-dependent DFT (TDDFT) was adopted for all the single-point excited-state calculations for optical absorption spectrum and

also the excited-state geometry optimization. Emission spectrum of H_2TTDC was obtained from the vertical excitations at the solvated optimized emissive state geometry (i.e., the lowest singlet excited-state). Long-range corrected RSH adopted in this study was proven very successful in describing physically meaningful frontiers orbitals, and also the valence and charge-transfer excitations.[3] All optimized geometries were confirmed to represent stationary points at the corresponding potential energy surface through harmonic normal mode analysis. All electronic structure calculations were performed using Gaussian 16 software package.[4]

Broken-symmetry intrachain FM and interchain AFM spin configurations were found to be the lower energy magnetic state with a calculated FM exchange coupling (J_{FM}) of ~5.4 kcal mol^{-1}. The sign of relatively weak J_{FM} is in accordance with the Goodenough-Kanamori rule.[5] This rule qualitatively suggests a weak FM super-exchange magnetic interaction between transition metal ions (here Co^{2+}) in insulators, connected via oxygen p-orbital of water molecule with a nearly orthogonal orientation ($\angle Co - O - Co = $ ~100° for the present case). An unpaired electron was localized at each of the Co^{2+} sites. Further, the calculated binding energy (E_b) of -28.34 kcal mol^{-1} clearly indicated a stable complex formation between the DCN and MOF structure with a stacking distance of ~3.4 Å and van der Waals (E_{vdW}) contributions of -15.50 kcal mol^{-1}.

Crystallographic Data and Structure Refinements:

Good quality single crystal of **IITKGP-80** MOF was sorted out with the help of a polarizing microscope and immersed in paratone oil, which was then mounted on the tip of glass fiber and cemented using epoxy resin. The single-crystal XRD diffraction data were collected at 298 K on a Bruker AXS (D8 Quest System) using graphite-monochromated *Mo*-K_α radiation (0.71073 Å). The linear absorption coefficients, scattering factors for the atoms, and the anomalous dispersion corrections were taken from International Tables for X-ray Crystallography. Bruker Apex III software was used for data collection, unit cell measurements, absorption corrections, scaling, and integration.[7,8] The data were reduced and an empirical absorption correction was applied with the help of SAINTPLUS software and SADABS programs using XPREP, respectively.[9,10] The structures were solved by the direct method using SHELXL-2018 in the WinGx programs. The WinGx package of programs was used to carry out the full-matrix least-squares refinement against the function $|F^2|$.[11,12] For all the cases, non-hydrogen atoms were refined anisotropically. All hydrogen atoms were geometrically fixed using the riding atom model and assigned fixed isotropic displacement parameters. The H atoms of the water molecules are assigned from the electron density map.

The "ACTA" command was used to generate the Crystallographic Information File (CIF). The structural details of the compound are presented in **Table S1**. CCDC: **2536337** contains the crystallographic data for **IITKGP-80**. These data are available from The Cambridge Crystallographic Data Center (CCDC) *via* www.ccdc.cam.ac.uk/data_request/cif.

Materials and reagents. $Co(NO_3)_2 \cdot 6H_2O$ (Merck), (Alfa Aesar), 4,4'-Dipyridyl disulfide (TCI) and organic solvents were used without further purification. The ligand (H_2TTDC), was prepared according to the previous literature method.[6] DCN (sigma) and other Orgnochlorine pesticides (SRL and Spectrochem) and organic solvents were used as obtained, without further purification.

Synthesis of IITKGP-80. A mixture of H_2TTDC (0.05 mmol, 1.0 equiv), DPS (4,4'-Dipyridyl disulfide) (0.05 mmol, 1.0 equiv), $Co(NO_3)_2 \cdot 6H_2O$ (0.06 mmol, 1.0 equiv), N,N'-dimethyl formamide (2 mL) and Methanol (1 mL) were added into a vial, which was kept at room temperature for slow evaporation. Red octahedron-shaped crystals were appeared after 15 days and collected by filtration.

Stability test of IITKGP-80. The MOF crystals were powdered and then the powdered bulk samples were dipped in the water, acidic and basic solutions, and various organic solvents for 24 h, thereafter filtered and dried under vacuum. The dried samples were analyzed with the help of PXRD analysis.

Sensing Experiments: The PXRD analysis confirmed the excellent hydro-stability of **IITKGP-80**. Thus, all the sensing experiments were performed in aqueous medium. The standard solution was prepared by adding a finely ground sample of **IITKGP-80** (1 mg) in 2 mL water and treated by ultrasonication for about 30 min. Different metal ions including Hg_2^{2+}, Hg^{2+}, Al^{3+}, Cr^{3+}, Zn^{2+}, Ni^{2+}, Cd^{2+}, Li^{+}, K^{+}, and Na^{+} with 10^{-2} M concentration were prepared in water. For making solution of Hg_2^{2+}, 56 milligrams of mercurous nitrate were dissolved ~ in 0.2 mL of 0.3 N nitric acid and diluted appropriately with water to prepare the analyte solutions with concentrations 10^{-2} M. The other metal ions were directly dissolved in water. Meanwhile, acetonitrile solutions of the organochlorine pesticides including 2,6-dichloro-4-nitroaniline (DCN), chlorobenzene (CB), 1,2-dichlorobenzene (1,2-DCB), 1,3-dichlorobenzene (1,3-DCB), 1,4-dichlorobenzene (1,4-DCB), 1,3,5-trichlorobenzene (1,3,5-TCB) and 1,2,4-trichlorobenzene (1,2,4-TCB) were prepared with a concentration of 10^{-2} M. For the luminescent-based titration experiments 2 mL dispersed solution of **IITKGP-80** was taken in

the cuvette with the gradual addition of the stock solution of analytes and the corresponding PL intensity was recorded. To verify the effectivity of MOF sensing over bared employed fluorogenic organic ligand (H_2TTDC), the luminescent quenching study was performed in aqueous medium by dispersing 1 mg ligand in 2 ml DMF (highly soluble in DMF), similar to the aqueous medium MOF dispersion.

Confirmatory Tests for Hg_2^{2+}: Three confirmatory tests were performed to confirm the stability of Hg(I) under the sensing experimental conditions. The addition of ammonia solution to the Hg(I) test solution, resulted black coloured precipitate, whereas when ammonia solution was added to the Hg(II) test solution, appearance of white precipitate was observed. Notably, this difference in observation for Hg(I) and Hg(II) clearly shows that Hg(I) does not undergo disproportionation under the experimental condition.[13] Further, the slow addition of potassium iodide in cold condition resulted the green precipitate of Mercury (I) iodide (Hg_2I_2) indicating the presence of Hg_2^{2+} as a dominant species in the analyte solution for sensing analysis. On the other hand, red precipitate of HgI_2 was obtained upon addition of KI to the Hg^{2+} analyte solution showing the clear distinction.[13] Furthermore, we have performed another test to validate the presence of Hg_2^{2+} as a dominant species in the prepared analyte solution. This characteristic test for Hg_2^{2+} (mercurous ion) involves adding excess thiocyanate along with ferric ions, where the mercurous ions reduce ferric ions to ferrous ions. The presence of ferrous ions is then detected using o-phenanthroline, after masking the ferric thiocyanate complex with fluoride. A distinctive red precipitate, extractable in amyl alcohol, confirms the presence of Hg_2^{2+} as a dominant species. Notably Hg^{2+} do not result a positive test.[14]

Stern-Volmer quenching constant (K_{sv}) and LOD calculations for Hg_2^{2+}, Hg^{2+} and DCN:

From the stock solution, the metal ions and pesticide analytes were successively added to the blank dispersed MOF suspension, and luminescence spectra were recorded until the complete luminescence quenching was observed. To get the quantitative estimation of the quenching efficiency, the individual luminescence titration profiles were fitted to the Stern–Volmer equation, $I_0/I = K_{sv}[M] + 1$; where I_0 and I denote the luminescence intensity of the water dispersed solution of **IITKGP-80** before and after the addition of the stock solution of the Hg_2^{2+}, Hg^{2+} and DCN, K_{sv} (M^{-1}) and [M] implies the concentration of the added analytes and quenching constant, respectively. The fitting was performed at a lower concentration, which displayed an excellent linear relationship with good linear fit correlation coefficient.

Considering the standard deviation (σ) *via* repeated luminescence measurements of the blank MOF solutions and based on the K_{sv} value, LOD values were calculated by the ratio of $3\sigma/K_{sv}$.

Quenching efficiency calculation:

The maximum quenching efficiency was calculated using $(1 - I/I_0) \times 100\%$ equation in which I and I_0 denote the recorded emission intensities after and before the analyte addition, respectively.

Recycling process:

The reusability of the luminescence sensing performance of **IITKGP-80** toward the targeted analytes was examined for up to five cycles for metal ions and DCN. For checking the recyclability, **IITKGP-80** was centrifuged after each luminescence titration experiment followed by washing with water and acetone repeatedly and then dried in air. The probe showed outstanding recovery of the initial luminescence intensity, even after six consecutive cycles of luminescence sensing experiments. As verified by the PXRD experiment, the MOF material retained the initial crystallinity after five successive cycles for each luminescence titration experiment.

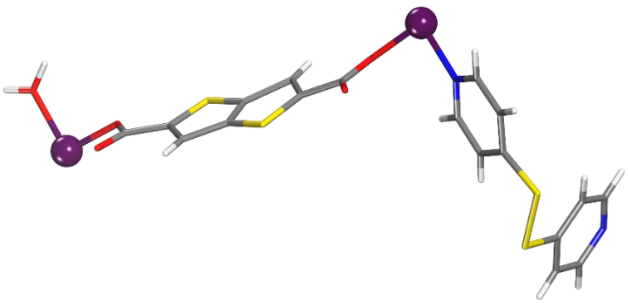

Figure S1: Asymmetric unit of **IITKGP-80.** Colour code: Co, Purple; N, light blue; O, red; S, Yellow; C, grey; H, white.

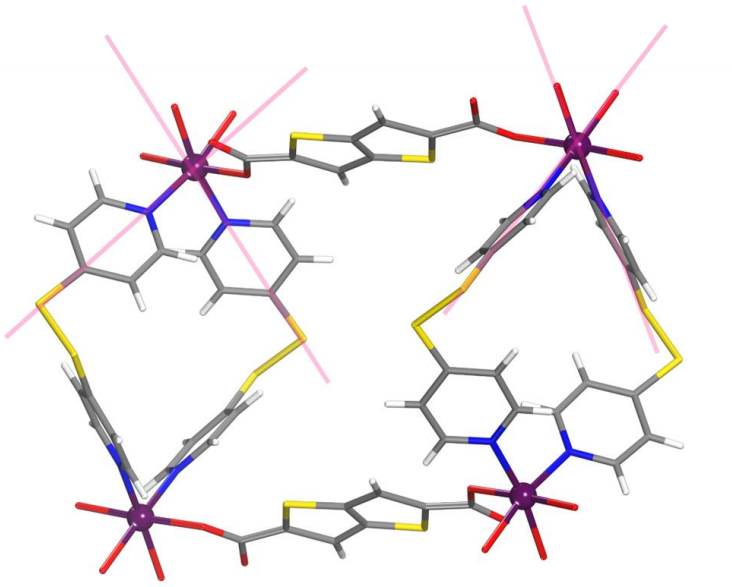

Figure S2: Variation of orientation of the DPS units of **IITKGP-80**. Colour code: Co, Purple; N, light blue; O, red; S, Yellow; C, grey; H, white.

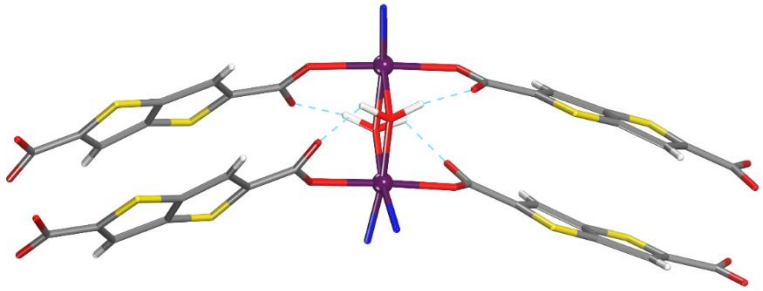

Figure S3: H-bonding interactions of **IITKGP-80**. Colour code: Co, Purple; N, light blue; O, red; S, Yellow; C, grey; H, white.

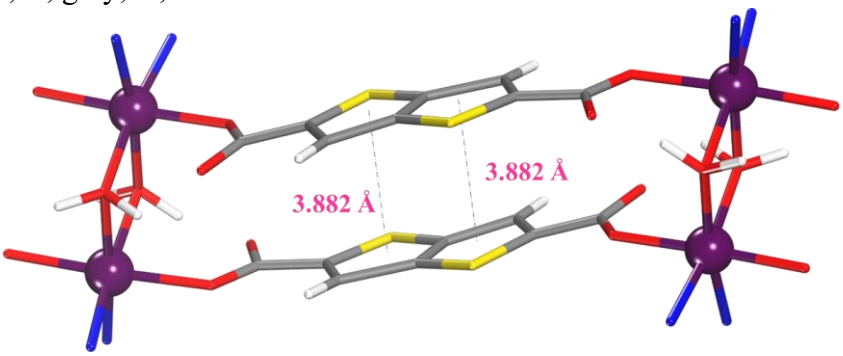

Figure S4: π···π stacking interactions of **IITKGP-80.** Colour code: Co, Purple; N, light blue; O, red; S, Yellow; C, grey; H, white.

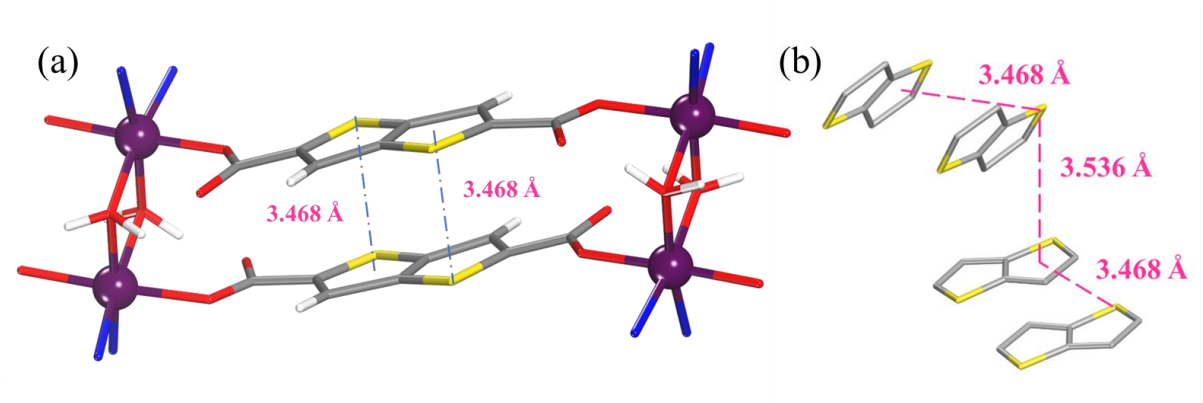

Figure S5: S···π interactions of **IITKGP-80.** Colour code: Co, Purple; N, light blue; O, red; S, Yellow; C, grey; H, white.

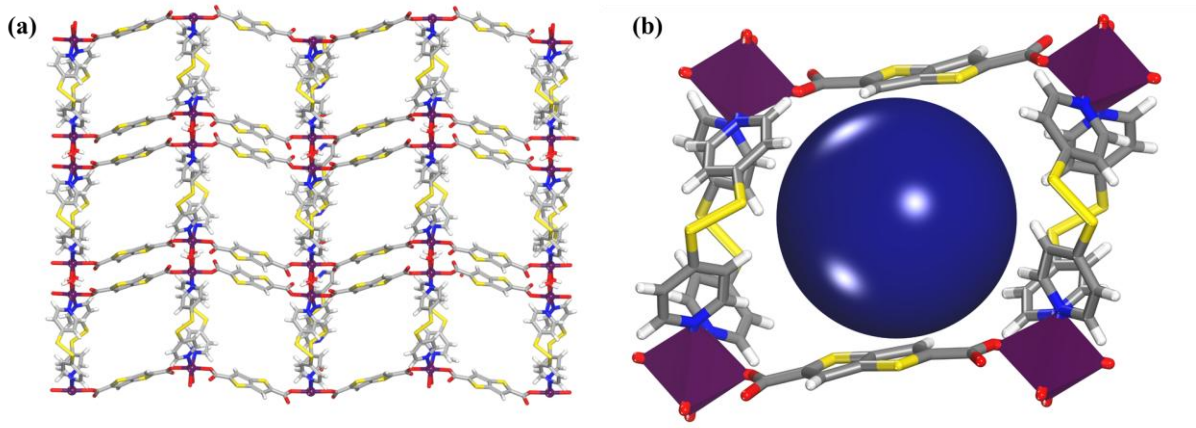

Figure S6: (a) A single 2D layer of **IITKGP-80**; (b) Pores present in a single 2D layer. Colour code: Co, Purple; N, light blue; O, red; S, Yellow; C, grey; H, white.

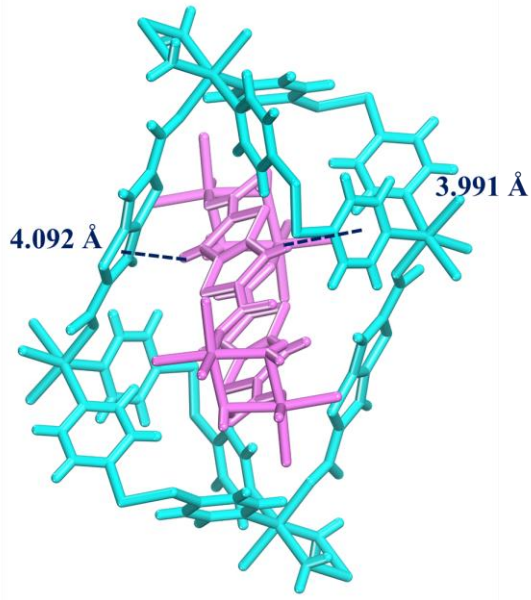

Figure S7: C-H···π interactions **IITKGP-80**.

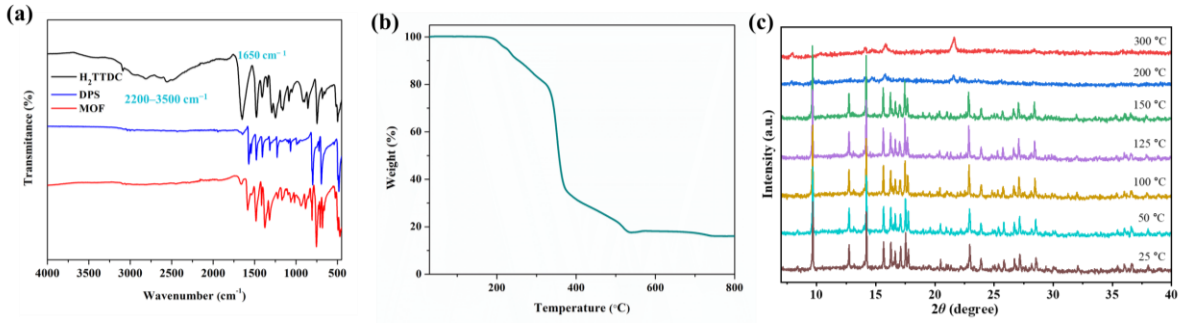

Figure S8: (a) IR-Spectra plot of the MOF: **IITKGP-80** and its constituent ligands; (b) Thermogravimetric analysis (TGA) profile for **IITKGP-80**; (c) VTPXRD-Analysis of **IITKGP-80**.

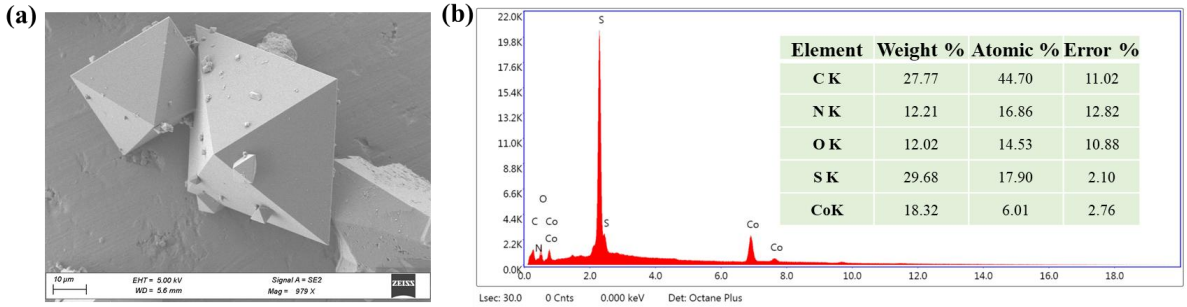

Element	Weight %	Atomic %	Error %
C K	27.77	44.70	11.02
N K	12.21	16.86	12.82
O K	12.02	14.53	10.88
S K	29.68	17.90	2.10
CoK	18.32	6.01	2.76

Figure S9: Microscopic analysis (a) SEM image and (b) EDS spectra of **IITKGP-80**.

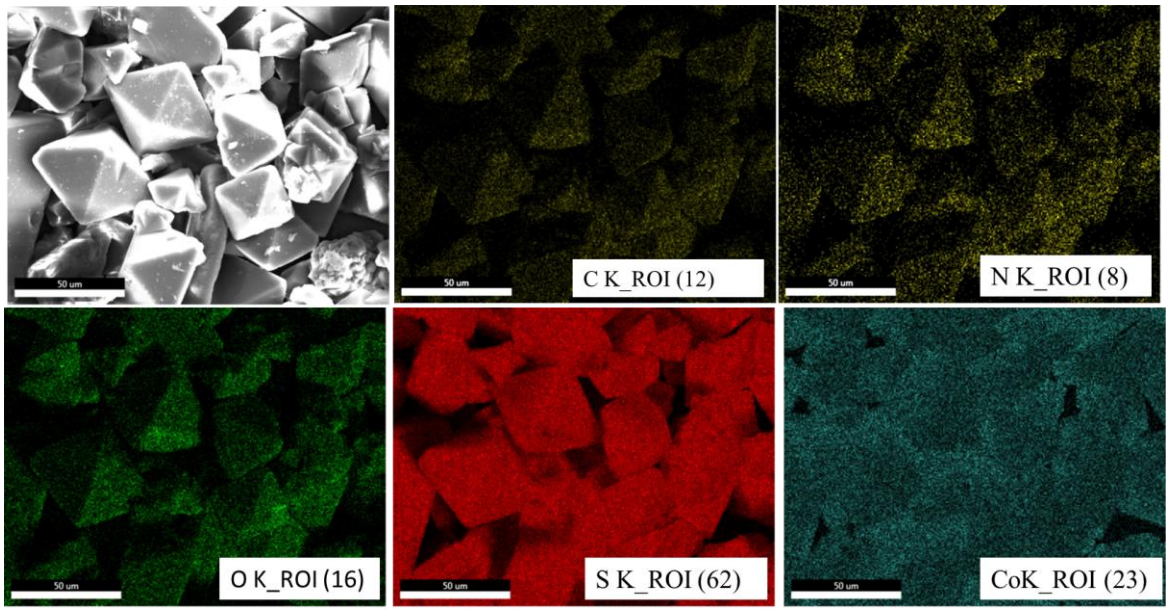

Figure S10: Elemental mapping of **IITKGP-80**.

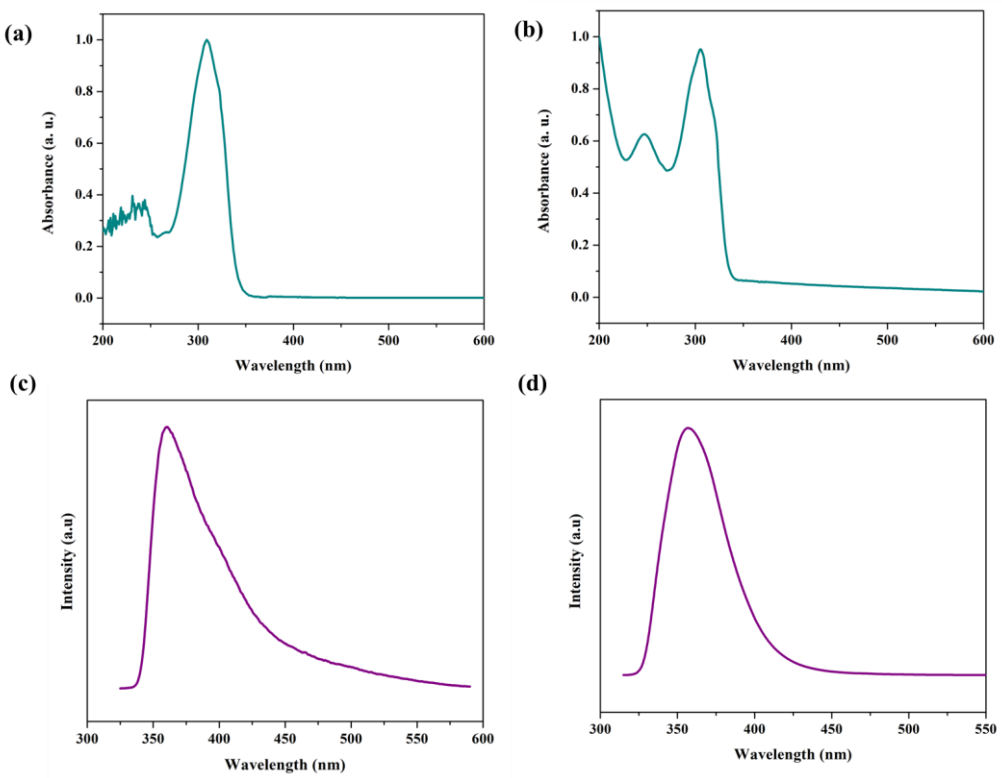

Figure S11: Solution state UV for (a) **H_2TTDC**, and (b) MOF: **IITKGP-80**; Solution state PL (photoluminescence spectra) of (c) **H_2TTDC** and (d) **IITKGP-80**

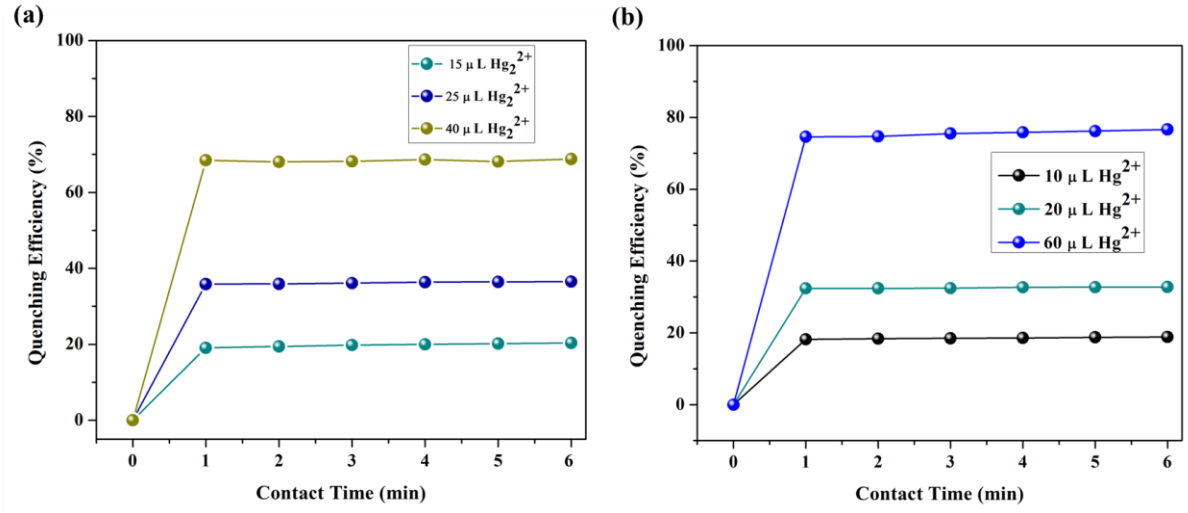

Figure S12: Kinetic plots for (a) Hg_2^{2+} and (b) Hg^{2+} sensing, respectively.

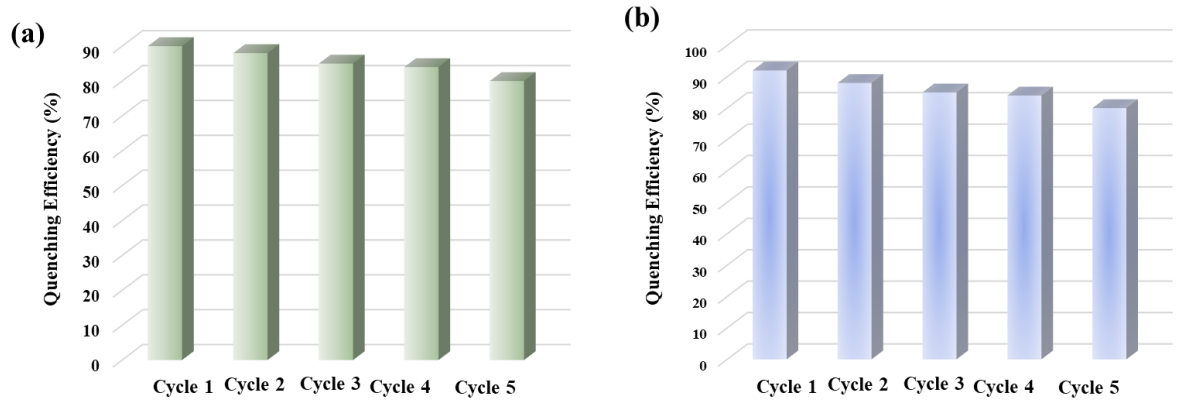

Figure S13: Recyclability performance of **IITKGP-80** for sensing of (a) Hg_2^{2+} and (b) Hg^{2+}.

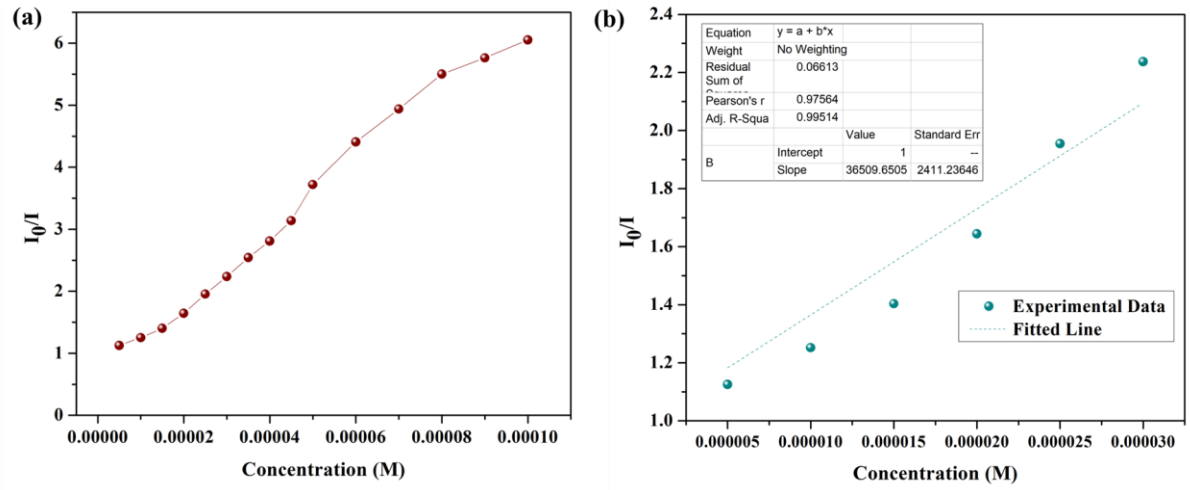

Figure S14: (a) Stern−Volmer plot for **IITKGP-80** with a gradual increase in the concentration of DCN pesticides; (b) linear region of luminescence intensity of probe in the low concentration range upon addition of DCN pesticide.

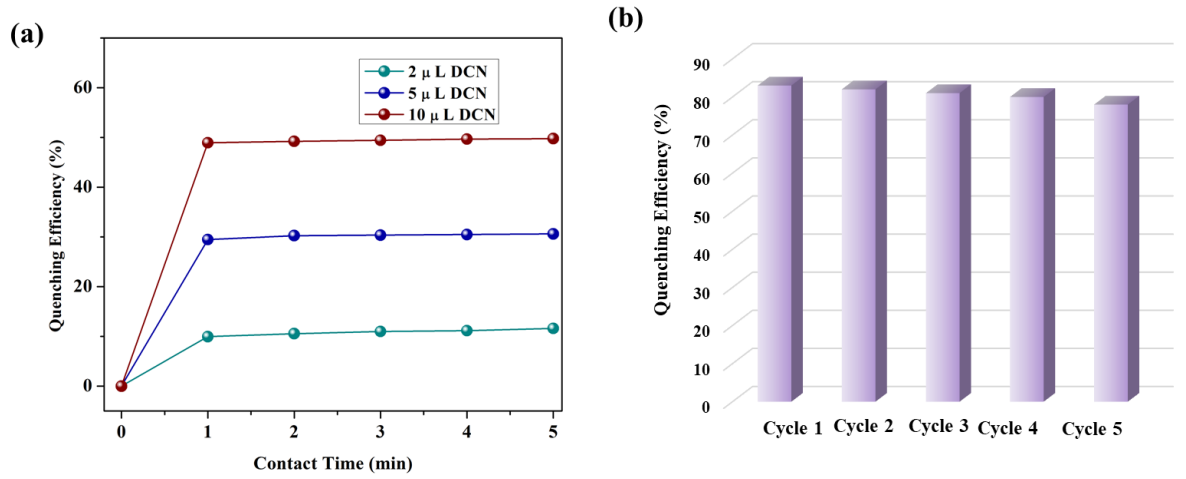

Figure S15: (a) Kinetic plots for DCN sensing, (b) Recyclability performance of **IITKGP-80** for sensing of DCN.

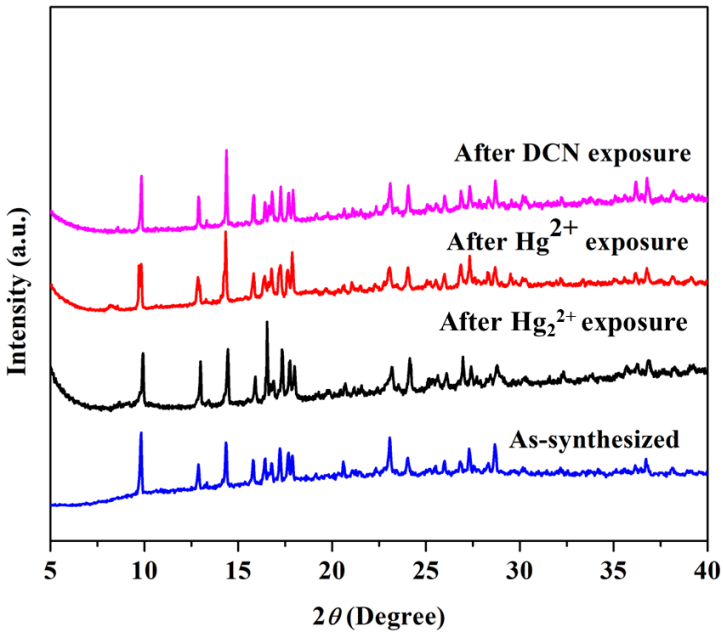

Figure S16: (a) PXRD comparison of **IITKGP-80** after Mercury and DCN sensing.

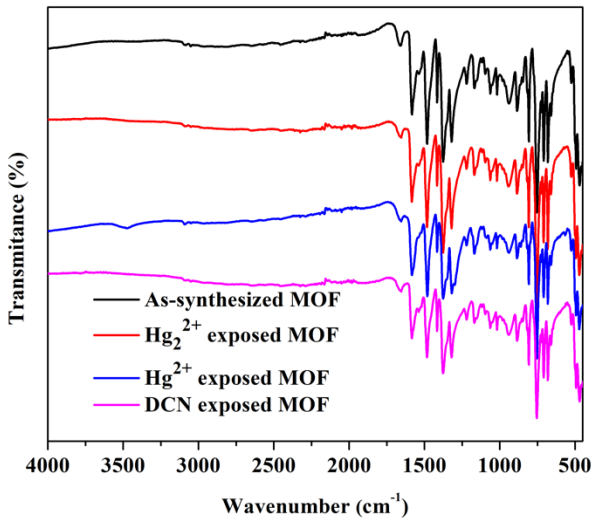

Figure S17. IR spectra of MOF: **IITKGP-80**, and after exposer to different aqueous analytes solution (Hg_2^{2+}, Hg^{2+} and DCN).

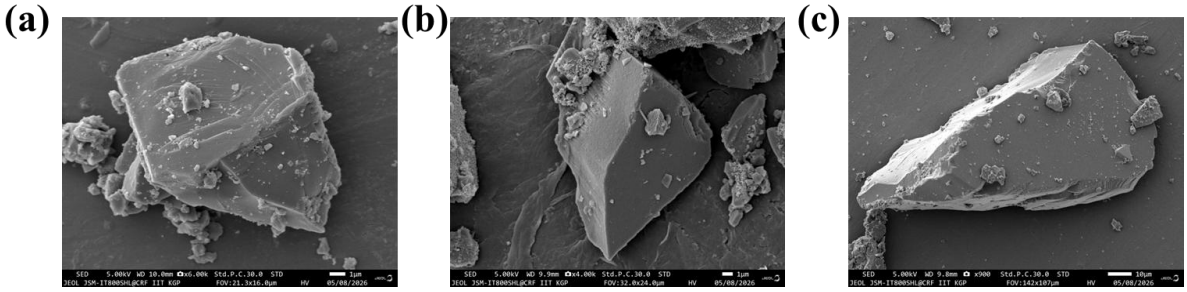

Figure S18. SEM Image of MOF: **IITKGP-80**, and after exposer to different aqueous analytes solution; (a) Hg_2^{2+}, (b) Hg^{2+} and (c) DCN.

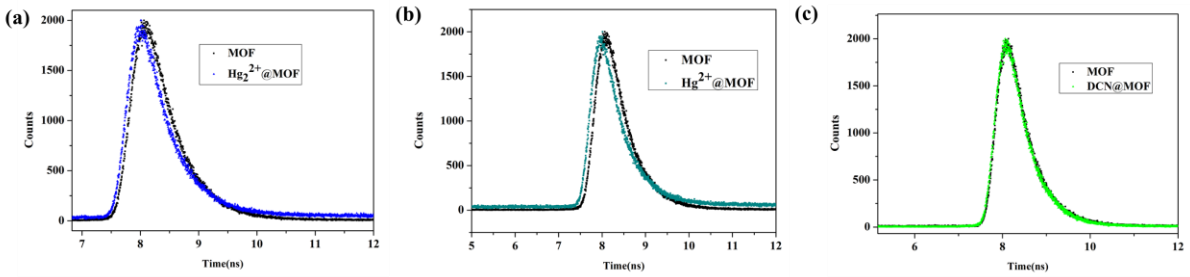

Figure S19: The lifetime decay plot of compound MOF: **IITKGP-80** before and after adding Hg(I), Hg(II) ion and DCN.

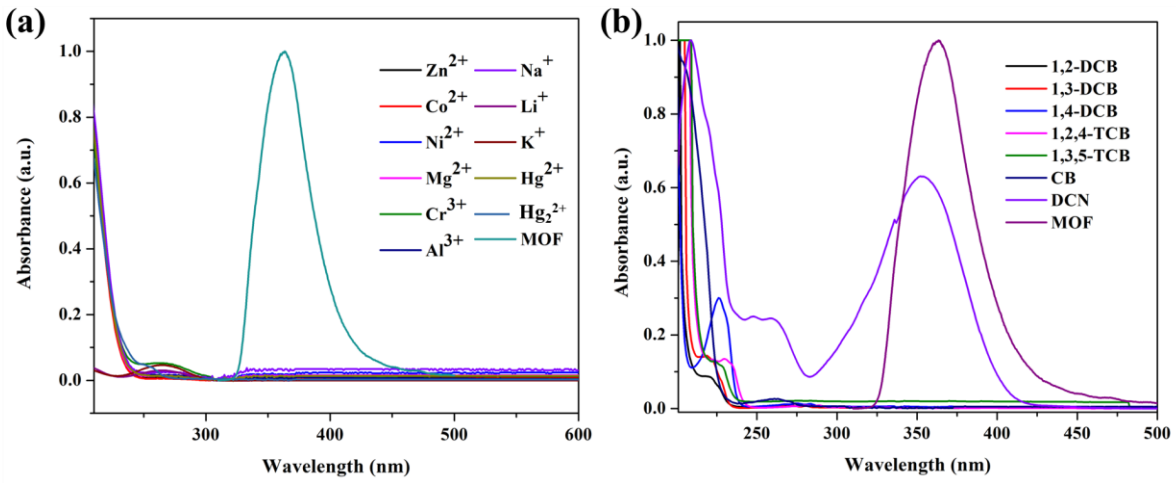

Figure S20: Spectral overlap between absorption spectra of (a) metal ions and (b) pesticides and emission spectrum of **IITKGP-80**.

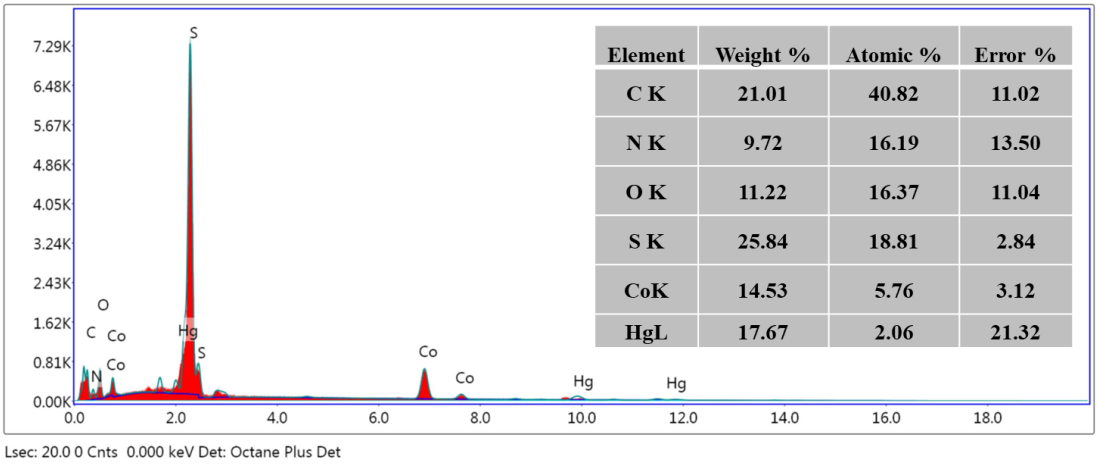

Element	Weight %	Atomic %	Error %
C K	21.01	40.82	11.02
N K	9.72	16.19	13.50
O K	11.22	16.37	11.04
S K	25.84	18.81	2.84
CoK	14.53	5.76	3.12
HgL	17.67	2.06	21.32

Figure S21: EDX spectrum of **IITKGP-80** after treatment with Hg_2^{2+} solution.

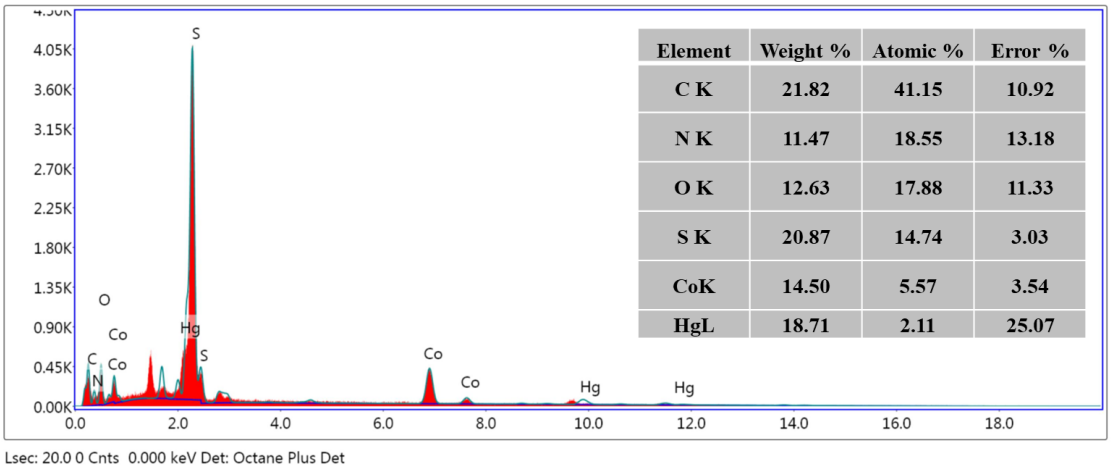

Element	Weight %	Atomic %	Error %
C K	21.82	41.15	10.92
N K	11.47	18.55	13.18
O K	12.63	17.88	11.33
S K	20.87	14.74	3.03
CoK	14.50	5.57	3.54
HgL	18.71	2.11	25.07

Figure S22: EDX spectrum of **IITKGP-80** after treatment with Hg^{2+} solution.

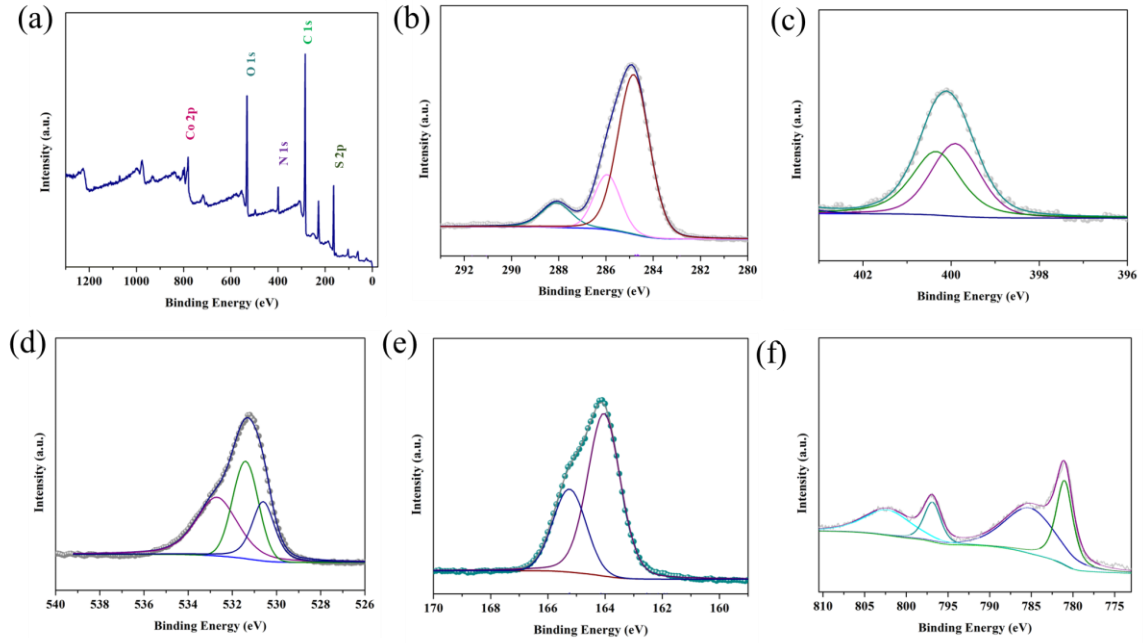

Figure S23: (a) Survey Scan; XPS fitted XPS spectra of (b) C (1s), (c) N (1s), (d) O (1s), (e) S (2p), (f) Co (2p) for **IITKGP-80**.

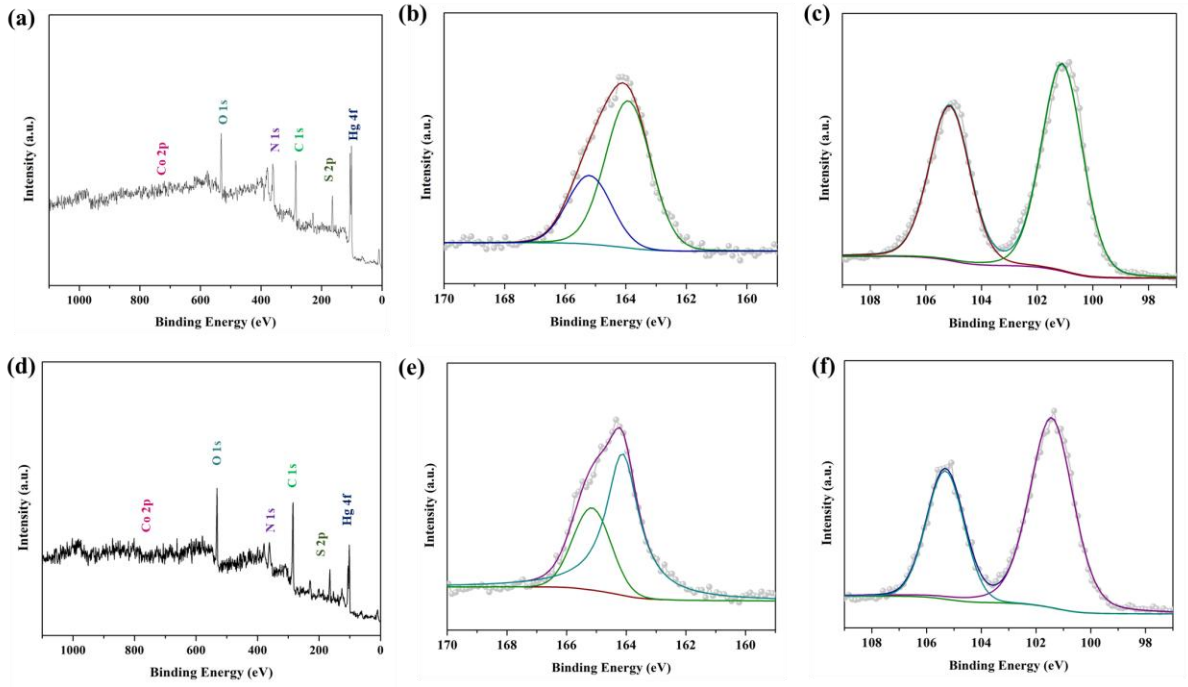

Figure S24: (a) Survey spectra; XPS fitted XPS spectra of (b) S (2p), (c) Hg (4f) of Hg_2^{2+} exposed **IITKGP-80**; (d) Survey spectra, (e) S (2p), (f) Hg (4f) for Hg^{2+} exposed **IITKGP-80**.

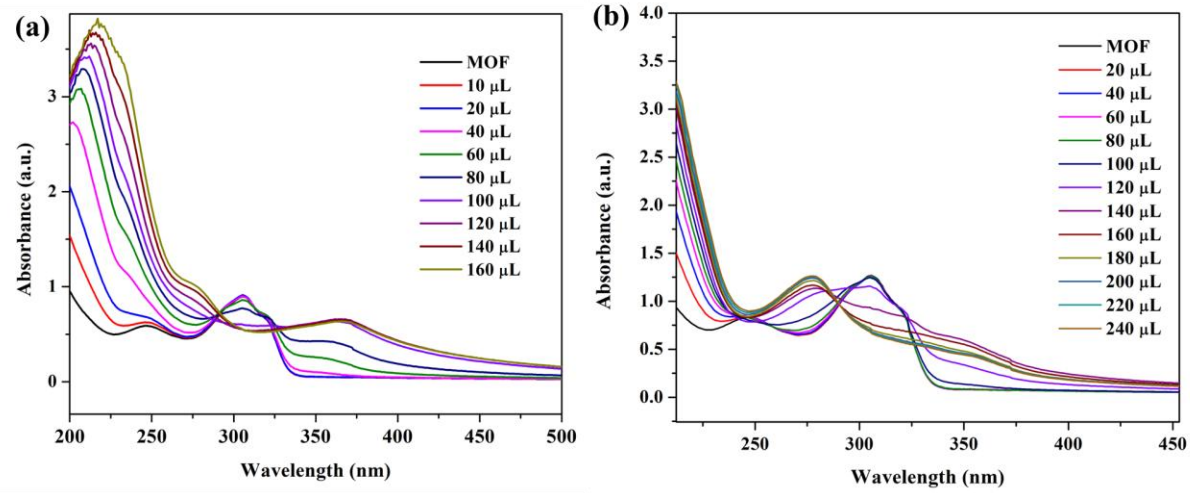

Figure S25: UV-Vis spectra of **IITKGP-80** upon addition of (a) Hg_2^{2+}, (b) Hg^{2+} solution (10^{-2} M).

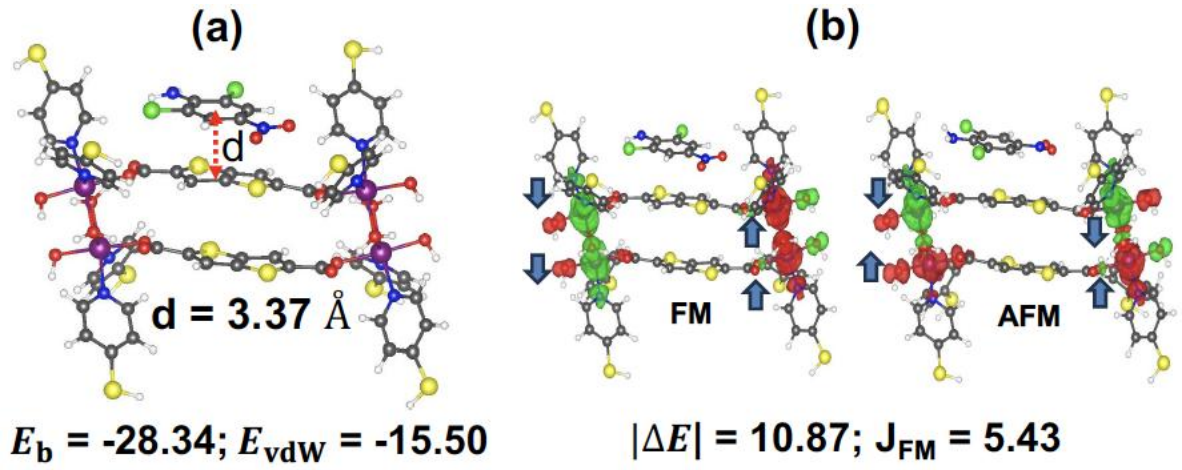

Figure S26: DFT optimized structure (a), spin-density iso-surfaces for the intrachain ferromagnetic (FM) and antiferromagnetic (AFM) spin configurations of DCN bound MOF (MOF@DCN) in water dielectric. Binding energy (E_b), van der Waals contribution (E_{vdW}) and energy differences between the FM (lowest energy state) and AFM spin configurations including magnetic exchange coupling (J_{FM}) are given in kcal mol^{-1}. Spin-density iso-surfaces are obtained with an iso-value of 0.001 electrons/Borh^3. White, grey, blue, red, yellow, green and purple coloured balls denote H, C, N, O, S, Cl and Co, respectively.

Table S1: Crystal data and structure refinements table.

Compounds	**IITKGP-80**
Empirical formula	C_{18} H_{12} Co N_2 O_5 S_4
Formula weight	523.47
Temperature (K)	131
Radiation	*Mo* (K_α)
Wavelength (Å)	0.71073
Crystal system	Orthorhombic
Space group	*Pnna*
a [Å]	13.393(3)
b [Å]	18.587(4)
c [Å]	16.729(4)
α [°]	90
B [°]	90
γ [°]	90
Volume [Å^3]	4164.3(15)
Z	8
Density (calculated) [g cm^{-3}]	1.670
Absorption coefficient [mm^{-1}]	1.259
F (000)	2120
Refl. used [$I > 2\sigma(I)$]	7467
Independent reflections	5277
R_{int}	0.0834
Refinement method	Full-matrix least-squares on F^2

GOF	1.117
Final *R* indices [$I>2\sigma(I)$]	R_1 = 0.0891, wR_2 = 0.2568
R indices (all data)	R_1 = 0.1264, wR_2 = 0.2908
CCDC	**2536337**

Table S2: Selected Bond Distances (Å) and Bond Angles (°) in **IITKGP-80**.

Co1 – O1	2.070(4)	Co1 – N1	2.124(5)
Co1 – Ow1	2.147(4)	Co2 – O3	2.081(4)
Co2 – N2	2.131(4)	Co2 – Ow1	2.139(4)

O1 – Co1 – O1	177.1(2)	N1 – Co1 – N1	94.9(2)
O1 – Co1 – N1	92.78(17)	O1 – Co1 – OW1	92.70(15)
O1 – Co1 – N1a	89.18(17)	O1 – Co1 – OW1a	85.07(15)
O1 – Co1 – N1b	89.19(17)	N1 – Co1 – OW1	92.75(16)
O1 – Co1 – N1c	92.78(17)	N1 – Co1 – OW1a	170.67(15)
OW1 – Co1 – OW1	80.2(2)		

Table S3: Hydrogen bonding interactions in **IITKGP-80**.

D-H…A	d(H…A) (Å)	d(D…A) (Å)	<DHA(°)
OW1 – H1W1 ... O4	1.820	2.481	124.11
OW1 – H1W2 ... O2	1.610	2.537	163.61

Table S4: Non-bonding interactions in **IITKGP-80**.

D-H…A	d(H…A) (Å)	d(D…A) (Å)	<DHA(°)
C15 – H15 ... O2	2.735	3.131	105.86
C13 – H13 ... O4	2.389	3.102	131.50

Table S5: Comparison table of K_{sv}, Limit of Detection (LOD) of previously reported MOFs for sensing of Hg^{2+} in aqueous medium.

Sl. No.	**Sensor**	**Sensing Medium**	**LOD (Hg^{2+})**	**LOD (Hg_2^{2+})**	**K_{SV} (Hg^{2+}, M^{-1})**	**K_{SV} (Hg_2^{2+}, M^{-1})**	**Reference**
1	**IITKGP-80**	**Water**	**1.05 µM**	**1.4 µM**	**4.5 ×10^3**	**3.3 ×10^3**	**This Work**
2	[Zn(2-NH_2bdc)(bibp)]$_n$	Water	---	--	4550	--	*Inorg. Chem.* **2015**, *54*, 7133–7135
3	Cd–EDDA	Water	0.002 µM	--	4.3 × 10^3	--	*Inorg. Chem.* **2015,** *54*,11046–11048

4	IITG-5a	Water	5.15 μM	--	3.54 × 10^5	--	*Inorg. Chem. Front.,* **2022,** *9*, 859
5	$[TbL_{1.5}(H_2O)_2]\cdot H_2O$	Water	--	--	7465	--	*Photochem. Photobiol. Sci.,* **2013**, *12*, 1700–1706
6	S, N-CD@Ce-MOF	Water	0.01 μM	--	--	--	*Anal. Methods*, **2024**, *16*, 3562–3576
7	$[Zn(L)(BBI)\cdot(H_2O)_2]$	Water	--	--	9390	--	*ACS Appl. Mater. Interfaces* **2017**, *9*, 15164−15175
8	$\{[Zn(4,4'\text{-}AP)(5\text{-}AIA)].(DMF)_{0.5}\}_n$	Water	9.9 × 10^{-12} M	--	1.011 × 10^9	---	*Inorg. Chem.* **2019**, *58,* 1377−1381
9	NIIC-3-Tb	Water	0.88 nM	--	1.29 × 10^7	-	*Angew. Chem. Int. Ed.* **2024**, *63*, e202410509
10	1, fluorescence probe pyrene-based derivatives	Water /DMF	0.42 μM	--	3.62 ×10^4 (Benesi-Hildebrand plot)	--	*Spectrochimica Acta Part A: Molecular and Biomolecular Spectroscopy* **2019**, *223,* 117315
11	(E)-N,N'-bis(4-(Z)-2-(4-butoxyphenyl)-1-cyanovinylphenyl)-1,4-benzenebismethaneimine (conjugated bis-Schiff base compound)	THF/ Water	0.24 μM	--		--	*Sensors and Actuators B* **2016**, *229,* 338–346
12	1, (4-[3-(4-hydroxyphenyl)-5-(2-thienly)-4,5-dihydro-pyrazol- 1-yl]benzenesulfonamide)	Water	14.54 μM	--	8.06 × 10^4	--	*Sensors and Actuators B* **2018**, *255,* 814–825
13	garlic extract stabilized AgNPs	Water	2 μM	--	--	--	*Colloids and Surfaces A* **2018**, *555*, 324–331
14	A-DMSA-UCNPs	DMSO/ Water	2.47 μM	--	--	--	*Sensors and Actuators: B.*

	A-PAA-UCNPs	DMSO/ Water	8.15 µM				*Chemical* **2021**, *326,* 128841
15	JUTH	DMF/ Water	15 µM	--	--	--	*Spectrochim. Acta, Part A* **2017**, *176,* 38–46.
16	mDTPES	THF/ Water	10 µM	--	--	--	*J. Mater. Chem. C,* **2018**,*6, 773-780*
17	L (A quinazoline derivative)	DMSO	6.34 µM	--	--	--	*Microchem. J.* **2019**, *150,* 104123.
18	Ag-PVA	Water	1 ppb	--	--	--	*ACS Appl. Mater. Interfaces* **2011**, *3,* 988–994.
19	Eu-Ca-MOF	Water	2.6 nM	--	--	--	*Talanta,* **2022**, *250,* 123710
20	Eu-MOF	Water	1.50×10^{-9} M	--	7.56×10^{5} M^{-1}	--	*Microchemical Journal,* **2024**, *196* 109712
21	Cj-3	Water	0.8083 ppm	--	2.87×10^{4} M^{-1}	--	*CrystEngComm,* **2024**, *26,* 5013-5029
22	PMP	DMSO: H_2O	5×10^{-8} M	--	4.5×10^{4} M^{-1}	--	*Scientific Reports,* **2025**, *15,* 33207

Table S6: Comparison table of K_{sv}, Limit of Detection (LOD) of previously reported MOFs for sensing of DCN in aqueous medium.

Sl. No.	DCN Sensor	Sensing Medium	LOD	Ksv (M^{-1})	Reference
1	**IITKGP-80**	**Water**	**0.13 µM**	**3.6×10^4 M^{-1}**	**This Work**
2	IITKGP-71	Water	0.21 µM	1.6×10^4	*Small* **2025**, *21*, 2409095
3	CSMCRI-9	Water	0.095 µM	4.96×10^4	*Mater. Chem. Front.* **2021**, *5*, 979.
4	Mg-APDA	DMF	0.725 µM	7.5×10^4	*Inorg. Chem.* **2018**, *57,* 13330.
5	$[Zn_3(DDB)(DPE)]\cdot H_2O$	Water	0.27 µM	3.3×10^4	*Dalton Trans.* **2019**, *48,* 16776.
6	CdMOF-1	Water	0.36 µM	4.93×10^4	*ACS Appl. Mater. Interfaces* **2023**, *15*, 6177.
7	CdMOF-2	Water	0.12 µM	2.03×10^4	
8	JXUST-12	EtOH	0.88 µM	4.75×10^4	Inorg. Chem. Front., **2022**,*9*, 1504-1513
9	$[Eu_2(dtztp)(OH)_2(DMF)(H_2O)_{2.5}]\cdot 2H_2O$	Water	25.5 µM	6.25×10^4	*Sensors and Actuators: B.*

					Chemical **2021**, *331*, 2021, 129377
10	$[Zn_2(bpdc)_2(BPyTPE)]$	DCM	0.63 μM	--	*Chem. Commun.*, **2017**, *53*, 9975-9978
11	$\{(Me_2NH_2)[In(BDPO)]\cdot DMF\cdot 2H_2O\}_n$	Water	18.60 μM	12×10^4 M^{-1}	*Inorg. Chem*. **2021**, *60*, 14, 10698–1070
12	Cd-CBCD	DMA	0.7 μM	4.47×10^4 M^{-1}	*Dalton Trans.*, **2019**, *48*, 2683 -2691
13	$[Ag(CIP^-)]$	DMF	0.17 μM	5.2×10^4 M^{-1}	*Dalton Trans.*, **2019**, *48*, 10892-10900
14	CdMOF-1 and CdMOF-2	DMF	--	--	*Appl. Organomet. Chem*., **2025**, *39, e70400*
15	MOF 3	Water	0.59 μM (123 ppb)	6.11×10^6 M^{-1}	*JACS Au* **2025**, *5,* 1875–1883
16	1@PMMA	--	1.18 μM	3.48×10^3 M^{-1}	*Talanta* **2024**, *277,* 126303
17	ACPP	Water	0.038 μM	3.8×10^5 M^{-1}	*Dyes and Pigments* **2024**, *222,* 111834
18	$[Ag_4(L)_2](PF_6)_4$ (1)	ACN	7.92 μM	4.51×10^4 M^{-1}	*Inorg. Chem.* **2024**, *63,* 2569–2576

Table S7. Detection of Hg_2^{2+} from tap water.

Hg_2^{2+} Spiked (mol L^{-1})	Hg_2^{2+} Found (mol L^{-1})	Recovery (%)	RSD (%) (n=3)
2.5×10^{-5}	2.56×10^{-5}	102.4	3.1
5×10^{-5}	5.05×10^{-5}	101	3.6
7.5×10^{-5}	7.25×10^{-5}	96.6	2.2

Table S8. Detection of Hg_2^{2+} from river water.

Hg_2^{2+} Spiked (mol L^{-1})	Hg_2^{2+} Found (mol L^{-1})	Recovery (%)	RSD (%) (n=3)
2.5×10^{-5}	2.48×10^{-5}	99.2	3.1
5×10^{-5}	4.87×10^{-5}	97.4	3.9
7.5×10^{-5}	7.24×10^{-5}	96.5	2.1

Table S9. Detection of Hg^{2+} from tap water.

Hg^{2+} Spiked (mol L^{-1})	Hg^{2+} Found (mol L^{-1})	Recovery (%)	RSD (%) (n=3)
2.5×10^{-5}	2.52×10^{-5}	100	2.9
5×10^{-5}	4.97×10^{-5}	99.4	2.1
7.5×10^{-5}	7.35×10^{-5}	98	2.1

Table S10. Detection of Hg^{2+} from river water.

Hg^{2+} Spiked (mol L^{-1})	Hg^{2+} Found (mol L^{-1})	Recovery (%)	RSD (%) (n=3)
2.5×10^{-5}	2.47×10^{-5}	98.8	2.8
5×10^{-5}	5.06×10^{-5}	101.2	3.6
7.5×10^{-5}	7.49×10^{-5}	99.86	1.5

Table S11. Detection of DCN from tap water.

DCN Spiked (mol L^{-1})	DCN Found (mol L^{-1})	Recovery (%)	RSD (%) (n=3)
2.5×10^{-5}	2.6×10^{-5}	104	2.39
5×10^{-5}	5.01×10^{-5}	100.2	1.50
7.5×10^{-5}	7.44×10^{-5}	99.2	2.8

Table S12. Detection of DCN from river water.

DCN Spiked (mol L^{-1})	DCN Found (mol L^{-1})	Recovery (%)	RSD (%) (n=3)
2.5×10^{-5}	2.46×10^{-5}	98.4	3.55
5×10^{-5}	5.01×10^{-5}	100.2	2.23
7.5×10^{-5}	7.58×10^{-5}	101	2.57

References:

[1] Chai, J.-D.; Head-Gordon, M. Long-range corrected hybrid density functionals with damped atom-atom dispersion corrections. *Phys. Chem. Chem. Phys.* **2008**, *10*, 6615-6620.

[2] Scalmani, G.; Frisch, M. J. Continuous Surface Charge Polarizable Continuum Models of Solvation. I. General Formalism. *J. Chem. Phys.* **2010**, *132* (11).

[3] Kronik, L.; Stein, T.; Refaely-Abramson, S.; Baer, R. Excitation gaps of finitesized systems from optimally tuned range-separated hybrid functionals. *J. Chem. Theory Comput.* **2012**, *8*, 1515-1531.

[4] Frisch, M. J. ea; Trucks, G. W.; Schlegel, H. B.; Scuseria, G. E.; Robb, Ma.; Cheeseman, J. R.; Scalmani, G.; Barone, V.; Petersson, G. A.; Nakatsuji, H. Gaussian 16. Gaussian, Inc. Wallingford, CT 2016.

[5] Goodenough, J. B. magnetism and the Chemical Bond. Interscience-Wiley, New York, 1963.

[6] C. Ma, L.-Y. Wang, M.-H. Shu, C.-C. Hou, K.-X. Wang, J.-S. Chen, *J. Mater. Chem. A* **2021**, *9*, 11530-11536.

[7] Sheldrick, G. M. Siemens Area Correction Absorption Correction Program; University of Göttingen: Göttingen, Germany, **1994**.

[8] Farrugia; L. J., WinGx suite for small-molecule single crystal crystallography. *J. Appl.Crystallogr.* **1999**, *32*, 837.

[9] SAINT+, 6.02ed, Bruker AXS, Madison, WI, **1999**.

[10] XPREP, 5.1 ed. Siemens Industrial Automation Inc., Madison, WI, **1995**.

[11] Sheldrick; G. M., SHELXL-97 Program for Crystal Structure Solution and Refinement; University of Göttingen: Göttingen, Germany, **1997**.

[12] Sheldrick, G. M. Crystal Structure Refinement with SHELXL. *Acta Cryst C* **2015**, *71*, 3–8.

[13] Svehla, G., & Sivasankar, B., *Vogel's qualitative inorganic analysis* (7th ed.). Pearson India Education.

[14] G. V. Ramesh and T. P. Radhakrishnan, *ACS Appl. Mater. Interfaces*, 2011, **3**, 988-994.